Journal of Molecular Modeling (2020) 26:287
https://doi.org/10.1007/s00894-020-04556-5

ORIGINAL PAPER

# The adsorption of chlorofluoromethane on pristine, and Al- and Ga-doped boron nitride nanosheets: a DFT, NBO, and QTAIM study

Mohsen Doust Mohammadi[1] · Hewa Y. Abdullah[2]

Received: 17 July 2020 / Accepted: 17 September 2020


## Abstract

In the present investigation, the feasibility of detecting the chlorofluoromethane (CFM) gas molecule onto the outer surface of pristine single layer boron nitride nanosheet (BNNS), as well as its aluminum (Al)– and gallium (Ga)–doped structures, was carefully evaluated. For achieving this goal, a density functional theory level of study using the Perdew, Burke, and Ernzerhof exchange–correlation (PBEPBE) functional together with a 6-311G(d) basis set has been used. Subsequently, the B3LYP, CAM-B3LYP, wB97XD, and M062X functionals with a 6-311G(d) basis set were also employed to consider the single-point energies. Natural bond orbital (NBO) and quantum theory of atoms in molecules (QTAIM) were implemented by using the B3LYP-D3/6-311G(d) method, and the results were compatible with the electronic properties. In this regard, the total density of states (TDOSs), the Wiberg bond index (WBI), natural charge, natural electron configuration, donor–acceptor natural bond orbital interactions, and the second-order perturbation energies are performed to explore the nature of the intermolecular interactions. All of the energy calculations and population analyses denote that by adsorbing of the gas molecule onto the surface of the considered nanostructures, the intermolecular interactions are of the type of strong chemical adsorption. Among the doped nanosheets, Ga-doped nanosheet has very high adsorption energy compared with other elements (i.e., Ga-doped > Al-doped > pristine). Generally, it was revealed that the sensitivity of the adsorption will be increased when the gas molecule interacts with decorated nanosheets and decrease the HOMO-LUMO band gap; therefore, the change of electronic properties can be used to design suitable nanosensors to detect CFM gas.

**Keywords** Chlorofluoromethane · CFM · Boron nitride · Nanosheet · Density functional theory · Freon 31 · Natural bond orbital

## Introduction

In the last two decades, theoretical studies in the density functional theory (DFT) framework on nanostructures have attracted the attention of many scientists in the fields of computational chemistry and solid-state physics [1–9]. The study of boron nitride nanosheet is no exception, and many theoretical studies on this nanostructure have led to interesting proposals for the manufacture of industrial devices [10–13]. Azizi et al. showed that when $H_2O$ molecule placed on the VD-8*8BNNS cavity, it will dissociatively chemisorbed [14]. Esrafili et al. have investigated widely various theoretical researches in order to adsorb different molecules such as NO [15], CO [16], $CH_2O$ [4], $COCl_2$ [17], $C_2H_4$ [18], and $N_2O$ [19] on the surface of pristine and decorated boron nitride nanosheet. Mohammadi et al. have studied the adsorption of halomethanes onto the BN, Al/Ga-doped nanosheets [7]. Rossini et al. showed the characterization of *h*-BNNS molecular edge terminations [20]. Shao et al. used BNNS@$Ti_3C_2$ as an electrocatalyst [21]. Joo et al. had an interesting simulation for the separation of copper and mercury using BNNS [22], and many other researches, all of which cannot be mentioned here [23–26]. The widespread use of boron nitride nanosheets provides the basis for further study on such structures.

Chlorofluoromethane (CFM) (also known as Freon 31 or HCFC 31 with chemical formula $CH_2ClF$) is classified as a category 2 carcinogen from the group of chlorofluorocarbons or dihalomethanes. It is a colorless, odorless, flammable gas

✉ Hewa Y. Abdullah
hewayaseen@gmail.com

[1] School of Chemistry, College of Science, University of Tehran, Tehran 14176, Iran

[2] Physics Education Department, Faculty of Education, Tishk International University, Erbil 44001, Iraq

Published online: 26 September 2020

with a solid monoclinic crystal structure of space group P21 [27]. Chlorofluoromethane was used as the refrigerant. It is listed in the Montreal Protocol as a substance that degrades the ozone layer [28]. A rotational study has been performed by Caminati et al. [29] to investigate the dimer interactions of CFM molecule, and the results confirm that the interactions are non-covalent. According to the dissociation energy of dimer complex of CMF molecule reported in [29], we considered it as an isolated single molecule in this work.

This article discusses the design of such a sensor. This study investigated the interactions of CFM with BNNS and BN nanosheets doped with Al and Ga elements. After optimizing the structure of boron nitride nanosheets by Gaussian software, to study the chemical stability and conductivity, the element doping process on this nanosheet has been studied. Because of the high sensitivity of computation to precisely determine the energy of molecular orbitals to investigate the conductivity and probability of physical and chemical adsorption, different structures need to be optimized using appropriate computational methods. For this purpose, the PBEPBE functional and 6-311G(d) basis set was used in this research for computation. The B3LYP, CAM-B3LYP, wB97XD, and M062X functionals with 6-311G(d) basis set were also used to calculate the single-point energies. Natural bond orbital and quantum theory of atoms in molecules were studied by using the PBEPBE/6-311G(d) method, and the results were used to obtain various physical parameters. Our results show that we can devise a gas sensor to detect CMF by using the pristine, and Al- and Ga-doped BNNS.

## Computational details

The DFT calculations at Perdew, Burke, and Ernzerhof (PBEPBE) functional [30] together with 6-311G(d) Pople split-valence triple-zeta basis set with polarization functions [31] were used for geometry optimization for all different positions of the CFM/sheet complex structures. To determine the stability of the optimized structures, frequency calculations are also performed using the similar level of theory to approve that all the stationary points are in agreement with a minimum point through the potential energy surface. For further investigation, single-point energy calculations using different levels of theory were also applied on the most stable relaxed structures, which were obtained from geometry optimization at the PBEPBE/6-311G(d) level. The levels of theory used for the single-point energy calculations included B3LYP-D3, M06-2X, and wB97XD together with 6-311G(d) basis set. Natural bond orbital (NBO) and quantum theory of atoms in molecules (QTAIM) were implemented by using the B3LYP-D3/6-311G(d) method. All of the calculations including geometry optimization, single-point energy calculations, and NBO analysis were performed by Gaussian 16 package [32]. It should be noted that the NBO calculations were performed using NBO v 3.0 software which is embedded within Gaussian software. In order to perform quantum theory of atoms in molecule (QTAIM) and density of state (DOS) analyses, the Multiwfn program [33–35] was employed.

The adsorption energy ($E_{ads}$) of the investigated CFM onto the surface of the pristine and doped nanosheets can be calculated as follows:

$$E_{ads} = E_{sheet/CFM} - (E_{sheet} + E_{CFM}) \quad (1)$$

where $E_{sheet/CFM}$ represents the total energy of the complex structure. $E_{sheet}$ and $E_{CFM}$ are the total energies of the pure nanosheet and the pure CFM molecule, respectively. Note that the absorption energy consists of two parts, namely the interaction energy ($E_{int}$) and the deformation energy ($E_{def}$) that occur in the absorption process. Therefore, the following equations are used to calculate these proportions:

$$E_{ads} = E_{int} + E_{def} \quad (2)$$

$$E_{int} = E_{sheet/CFM} - E_{sheetincomplex} - E_{CFMincomplex} \quad (3)$$

$$E_{def} = E_{def}^{sheet} + E_{def}^{CFM} = \left(E_{sheetincomplex} - E_{pristinesheet}\right) + \left(E_{CFMincomplex} - E_{isolatedCFM}\right) \quad (4)$$

where $E_{\text{sheet in complex}}$ and $E_{\text{CFM in complex}}$ are energies of CFM molecule and nanosheet in the optimized complexes, respectively.

## Results and discussion

### The structural analysis

To optimize the structure of pristine single layer boron nitride nanosheets using periodic boundary conditions, we select a 2D unit cell of boron and nitrogen atoms which is a = 10.0042 Å and b = 10.0043 Å in length containing 32 atoms. We optimized this nanosheet by DFT method with PBEPBE functional together with basis set 6-311G (d). After optimization of the pristine nanosheet, we substituted Al and Ga with B atom; then, the optimization process has been repeated for doped nanosheets. The quantitative values of bond lengths are shown in Fig. 1.

The next step was the optimization of CFM/nanosheet complexes. In this step the CFM molecule was placed on the outer surface of each abovementioned nanosheets with vertical distance of about 2.1 Å. To find out the optimum distances between nanosheet and CFM molecule, we used the rigid scan for some cases to estimate the most efficient distance. It should be noted that the level of theory in both optimization and rigid scan was PBEPBE/6-311G (d). To better explain the

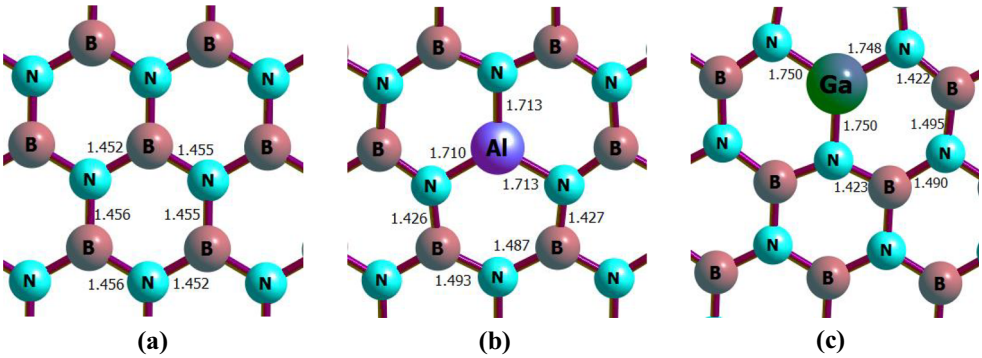


**Fig. 1** The values of bond length for **a** BNNS, **b** BNAlNS, and **c** BNGaNS. The optimization process has been done using PBEPBE/6-311G(d) level of theory. All values are in angstrom (Å)

details of the adsorption process, it will be useful to compare Figs. 1 and 2.

The boron nitride nanosheet is composed of several symmetric hexagons that have four different adsorption positions for the adsorption of any molecule onto the outer surface of the nanosheet as shown in Fig. 3: adsorption position on B atom ($T_1$); adsorption position on N atom ($T_2$); and adsorption position on B–N bond ($T_3$); adsorption position at hexagonal center ($T_4$). The logical approach is to put the CFM molecule in each of these positions and measure the amount of adsorption energy ($E_{ads}$). It is important to note that the CFM molecule has different heads (H, Cl, F), and each of these heads must be placed on the desired position on the nanosheet to measure the amount of absorption energy. Our experience shows that negligible differences exist in the amounts of adsorption energies when we place the CFM in any of the possible adsorption sites. As mentioned in [36], when the differences in the adsorption energies are "below the range of chemical interest," placing the gas in different positions on the nanosheets provides identical results. Nevertheless, we put the CFM molecule from F-head onto the desired positions on the BN nanosheet. The test result showed that there is a

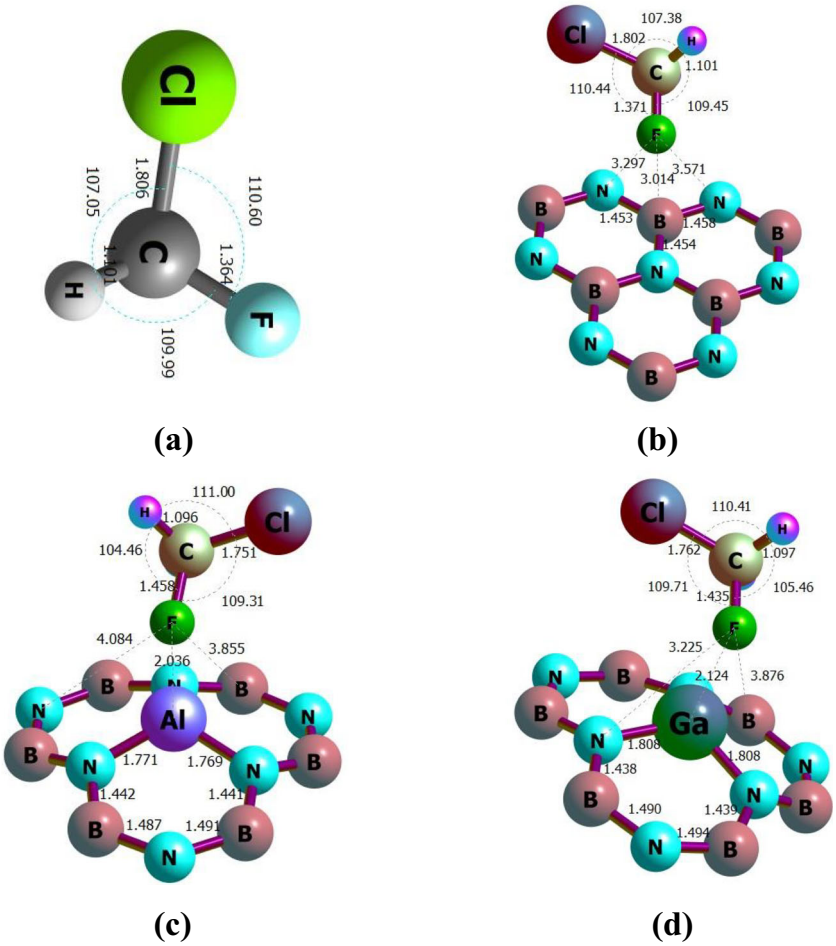


**Fig. 2** The most stable form of **a** isolated CFM and the adsorbed CFM molecule onto the outer surface of **b** BNNS, **c** BNAlNS, and **d** BNGaNS. All clusters have been optimized using the PBEPBE functional and 6-311G(d) basis set. All values are in angstrom (Å)

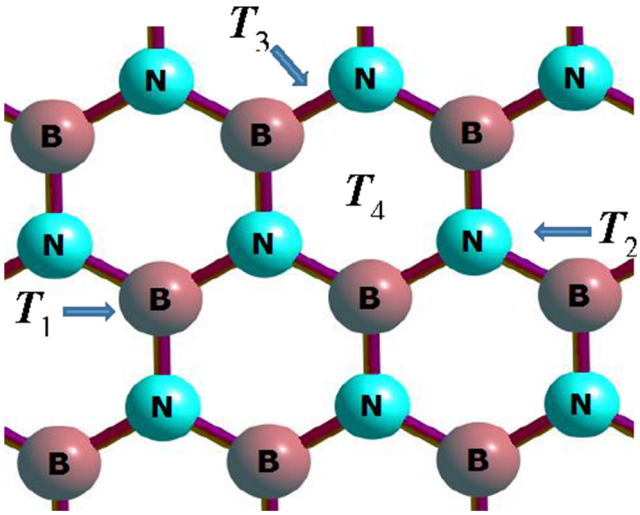


**Fig. 3** All possible target positions for the adsorption of any arbitrary molecules onto the surface of BNNS. Top of boron atom ($T_1$), top of nitrogen atom ($T_2$), between boron and nitrogen atoms ($T_3$), and top of the hexagonal ring ($T_4$)

negligible difference among the adsorption energies; therefore, the boron atom position was the target position on the BN nanosheet.

In the next step, the nanosheet is expanded three times in each direction (a = 25.85 Å, b = 25.92 Å) and terminated with hydrogen atom. Since the PBEPBE functional does not account for the scattering contribution, it is expected that in poor interactions, this functional will not give a good estimate of the amount of energy. For this reason, methods have been developed for effects. One of the most effective, accurate, and low computational methods is the experimental method developed by Grimme et al. This method is highly accurate because it has an empirical basis and its parameters are extracted from the spectroscopic experimental data. Various versions of the semi-empirical Grimme method have been presented in recent years [37–39]. In this work we used the latest version of B3LYP-D3 known as D3 (BD) (GD3BJ), and wB97XD to consider long range and dispersion effects.

Single-point energy calculations using different functional such as B3LYP-D3, wB97XD, and M062X and 6-311G(d) basis set were done. The calculated values indicate a strong interaction between nanosheets and CFM molecule. Since the PBE-PBE functional does not account for the long-range scattering contribution, it is expected that in poor interactions, this functional will not give a good estimate of the amount of energy. For this reason, methods have been developed for long range and dispersion effects. In this work we used B3LYP-D3 and wB97XD to consider long range and dispersion effects. The well-known M062X functional is used for better comparison. The results show that the energies obtained from the PBEPBE and other functionals are consistent with the accuracy of the calculations. On the other hand, as expected, the B3LYP-D3 method shows more energy values than the others, due to the dispersion contribution consideration. Also by doping the Al and Ga elements on the BN nanosheet, significant changes in the results are achieved. Table 1 shows that doping Al and Ga increases the absorption energy and enhanced the chemical absorption. Table 2 also shows the bond length and the nearest intermolecular distances (re (Å)) between CFM molecule and BNNS, BNAlNS, and BNGaNS (Fig. 4).

## Energetics properties

The chemical electron potential ($\mu$) describes the tendency of electrons to escape from a particular species at the ground state. This quantity is equal to the absolute negative electronegativity obtained from the definition provided by Mulliken, as follows:

$$\mu = -\chi \tag{5}$$

Parr and his colleagues [40] used the DFT to show that at a constant external potential, the potential energy of an electron is related to the first derivative of energy relative to the number of electrons, as follows:

$$\mu = \left(\frac{\partial E}{\partial N}\right)_{\upsilon(r)} = -\frac{1}{2}(IP + EA) \tag{6}$$

where $IP$ and $EA$ are the ionization affinity and electron affinity, respectively [41]. Based on the Koopmans' approximation (see the Hartree–Fock theory) and Janak's approximation [42] (in the DFT theory), the ionization and electron affinity potentials are equal to the negative value of the highest occupied molecular orbital (HOMO) energy ($\varepsilon_{HOMO} = -IP$) and negative value of the lowest unoccupied molecular orbital (LUMO) ($\varepsilon_{LUMO} = -EA$). Therefore, the chemical potential in Janak's approximation is defined as

$$\mu = \left(\frac{\partial E}{\partial N}\right)_{\upsilon\left(\vec{r}\right)} \cong \frac{(\varepsilon_{LUMO} + \varepsilon_{HOMO})}{2} \tag{7}$$

where $\varepsilon_{HOMO}$ and $\varepsilon_{LUMO}$ are the energies of the HOMO and the LUMO, respectively. $N$ is the number of electrons, $E$ is the total electronic energy of the system, and $\upsilon(r)$ is the external potential.

Comparison of the variation in electron chemical potentials to that in the number of electrons at a constant external potential is called chemical hardness, which is expressed as

$$\eta = \left(\frac{\partial \mu}{\partial N}\right) = \frac{1}{2}\left(\frac{\partial^2 E}{\partial N^2}\right) \tag{8}$$

Parr et al. [43] used the electron energy curve as well as the finite difference approximation to express hardness as follows:

**Table 1** The adsorption energies ($E_{ads}$) and deformation energies ($E_{def}$) for BNNS, BNAlNS, and BNGaNS with CFM molecule. All values are in (eV)

| Systems | PBEPBE | | B3LYP-D3 | | M06-2X | | wB97XD | |
|---|---|---|---|---|---|---|---|---|
| | $E_{ads}$ | $E_{def}$ | $E_{ads}$ | $E_{def}$ | $E_{ads}$ | $E_{def}$ | $E_{ads}$ | $E_{def}$ |
| $CH_2ClF$/BNNT | − 0.163 | 0.003 | − 0.386 | 0.011 | − 0.247 | 0.009 | − 0.364 | 0.015 |
| $CH_2ClF$/BN(Al)NT | − 1.043 | 0.021 | − 1.330 | 0.031 | − 1.195 | 0.018 | − 1.270 | 0.028 |
| $CH_2ClF$/BN(Ga)NT | − 1.085 | 0.027 | − 1.342 | 0.025 | − 1.343 | 0.029 | − 1.280 | 0.035 |

$$\eta = \frac{1}{2}(IP - EA) \tag{9}$$

Moreover, using Janak and Koopman's approximations, the hardness equation is transformed as follows:

$$\Delta E_{min} = -\frac{\mu^2}{2\eta} \tag{10}$$

Chemical hardness is the energy gap between the HOMO and the LUMO. Therefore, molecules with high energies are considered hard molecules, while those with low energies are called soft molecules. Since the softness of a molecule is the opposite of its hardness, the equation for molecule softness is denoted as follows [44]:

$$S = \frac{1}{\eta} \tag{11}$$

Inspired by Maynard's work, Parr et al. [45] introduced electrophilicity as the steady-state energy in which an atom or a molecule at ground state gains by receiving additional electron charges from the environment. The energy changes that lead to such a charge transfer are expressed as follows:

$$\Delta E = \mu \Delta N + \frac{1}{2}\eta(\Delta N)^2 \tag{12}$$

When the system receives electron charges from the environment sufficient to equate its potential to that of the environment, the system is saturated with electrons and can be expressed as follows:

**Table 2** The bond lengths and the nearest intermolecular distances (re (Å)) between CFM molecule and BNNS, BNAlNS, and BNGaNS. All calculations were performed using PBC-DFT PBEPBE/6-311G(d) level of theory (x = Al and Ga)

| Systems | F.... (x) | F....B | F....N | C–F | C–Cl | C–H |
|---|---|---|---|---|---|---|
| $CH_2ClF$/BNNS | - | 3.014 | 3.297 | 1.371 | 1.802 | 1.101 |
| $CH_2ClF$/BNAlNS | 2.036 | 3.855 | 4.084 | 1.458 | 1.751 | 1.096 |
| $CH_2ClF$/BNGaNS | 2.124 | 3.876 | 3.225 | 1.435 | 1.762 | 1.097 |

$$\frac{d\Delta E}{d\Delta N} = 0 \tag{13}$$

The electron load received from the environment is maximized, and the total energy of the system is eventually minimized. Thus,

$$\Delta N_{max} = -\frac{\mu}{\eta} \tag{14}$$

$$\Delta E_{min} = -\frac{\mu^2}{2\eta} \tag{15}$$

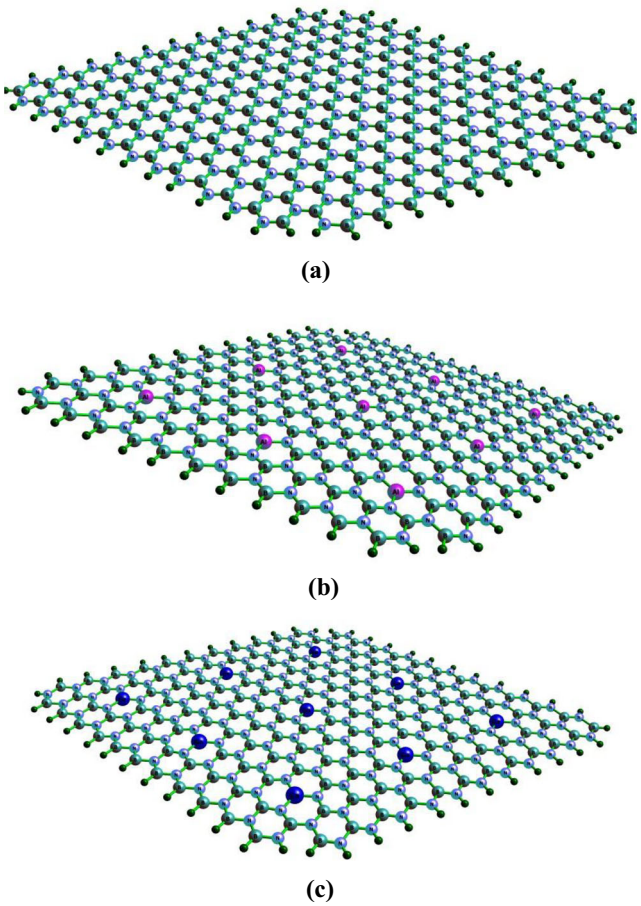

**Fig. 4** The 2D **a** boron nitride, **b** Al-doped boron nitride, and **c** Ga-doped boron nitride nanosheets terminated with hydrogen atoms

Since $\eta > 0$, $\Delta E < 0$ always, and the charge transfer is energetically desirable. Accordingly, Parr et al. proposed the following equation to denote the electrophilicity of electrophilic species.

$$\omega = \frac{\mu^2}{2\eta} \tag{16}$$

In fact, the electrophilicity index is the capacity of a species to accept an arbitrary number of electrons from the environment. In this regard, Nourizadeh and Maihami [46] used electrophilicity in the Diels–Alder reaction and stated that "atoms appear to be arranged in a natural tendency to reach the lowest electrophilicity." This expression is called the minimum electrophilicity principle (MEP).

The values of maximum occupied molecular orbital (HOMO) and lowest occupied atomic orbital (LUMO) and their differences (HLG), chemical potential ($\mu$), chemical hardness ($\eta$), and electrophilicity ($\omega$) are reported in Table 3. From the results of this table, it can be seen that by adsorption of CFM molecule onto the outer surface of nanosheets, the distance between HOMO and LUMO levels is reduced relative to the pure nanosheet, which shows the greatest decrease in the interaction of the Al-doped boron nitrogen nanosheet and CFM, which is caused by the molecular energy absorption matched from this position. By doping the elements Al and Ga, it is observed that HLG changed. The decrease in HLG results in an increase in the electrical conductivity and thus an increase in the metal property of all the nanosheets compared with pure BNNS. It is also noteworthy that the observed changes in HLG after doped Al and Ga are mainly due to lower LUMO energy levels. In order to study these changes in the electron structure of the studied cases more closely, the density of state spectra (DOS) will be analyzed in the next section. For a more detailed study of the electron structure changes, the density of state spectra (DOS) is extracted and illustrated in Fig. 5.

From the DOS spectra, it is clear that DOS spectra for all absorption are in agreement with the values of the energy parameters reported in Table 3. The lowest amount of adsorption energy is related to the pristine nanosheet, and the highest amount of adsorption energy is for the adsorption of CFM onto the Al-doped BN nanosheet; the most changes are also observed in the DOS spectrum relative to the Al-doped nanosheet. In other words, the electron structure changes show a direct relationship with the absorption energies. Given the amount of absorption energy, high amount of binding energy, and the structure of DOS spectra obtained in all of these cases, it can be claimed that the adsorption of CFM molecule onto BN, BN (Al), and BN (Ga) nanosheets is a strong physical adsorption type.

**Table 3** Values of HOMO energy ($\varepsilon_H$), LUMO energy ($\varepsilon_L$), HOMO and LUMO energy gap (HLG), chemical potential ($\mu$), chemical hardness ($\eta$), and electrophilicity ($\omega$). All values are in (eV) and were obtained from completed nanosheet B3LYP-D3/6-311G(d) level of theory

| Systems | $\varepsilon_H$ | $\varepsilon_L$ | HLG | $\mu$ | $\eta$ | $\omega$ |
|---|---|---|---|---|---|---|
| BNNS | − 6.374 | − 0.446 | 5.929 | − 3.310 | 2.864 | 15.692 |
| BNAlNS | − 6.177 | − 0.437 | 5.739 | − 3.307 | 2.870 | 15.692 |
| BNGaNS | − 6.180 | − 0.438 | 5.742 | − 3.309 | 2.871 | 15.716 |
| CBrClF2/BNNNS | − 6.355 | − 0.448 | 5.907 | − 3.301 | 2.854 | 15.550 |
| CBrClF2/BNAlNS | − 6.084 | − 0.541 | 5.543 | − 3.313 | 2.772 | 15.208 |
| CBrClF2/BNGaNS | − 6.105 | − 0.425 | 5.680 | − 3.265 | 2.840 | 15.137 |

## NBO and QTAIM analyses

The natural bond orbital (NBO) analysis has been developed based on many-electron molecular wavefunction in terms of localized electron-pair bonding units and uses first-order reduced density matrix of the wavefunction [47, 48]. In the NBO approach, a given wavefunction should be transformed into a localized form in which NBOs are considered local block eigenfunctions of the density matrix. NBO analysis is applicable in both closed-shell and open-shell systems which are calculated from atom-centered basis functions [49]. The mechanism of the energetic analysis of NBO interactions is based on the one-electron effective energy operator (Fock or Kohn–Sham matrix) that arises from the host electronic structure system (ESS). Second-order perturbation theory is one of the highest uses methods for estimating energy effects. For the case of HF or DFT methods, the interactions between NBOs are considered to analyze the wavefunction energetically, with the explanation that the Kohn–Sham matrix elements [50–60].

We used the B3LYP/ DEF2-QZVP level of theory to perform the NBO calculations. The concept of bonded orbitals can be used to understand the distribution of electrons in atomic and molecular orbitals. Atomic charges and molecular bonds can be used to obtain these orbitals. In this method, an electron density matrix is used to both define the shapes of the atomic orbitals in the molecular environment and obtain molecular bonds (electron density between atoms). NBO is defined as the following equation for $\sigma$ bonding between atoms A and B.

$$\sigma_{AB} = C_A h_A + C_B h_B \tag{17}$$

where $h_A$ and $h_B$ are natural hybrids on the A and B atoms. In the covalent limit, $C_A = C_B$, and at the ionic limit, $C_A >> C_B$ (if the electronegativity of A is greater than B). Each bonding NBO must be paired with a corresponding anti-bonding NBO.

$$\sigma^*_{AB} = C_A h_A - C_B h_B \tag{18}$$

Binding orbital analysis is used to evaluate the effects of non-stationary effects, such as anomeric effect,

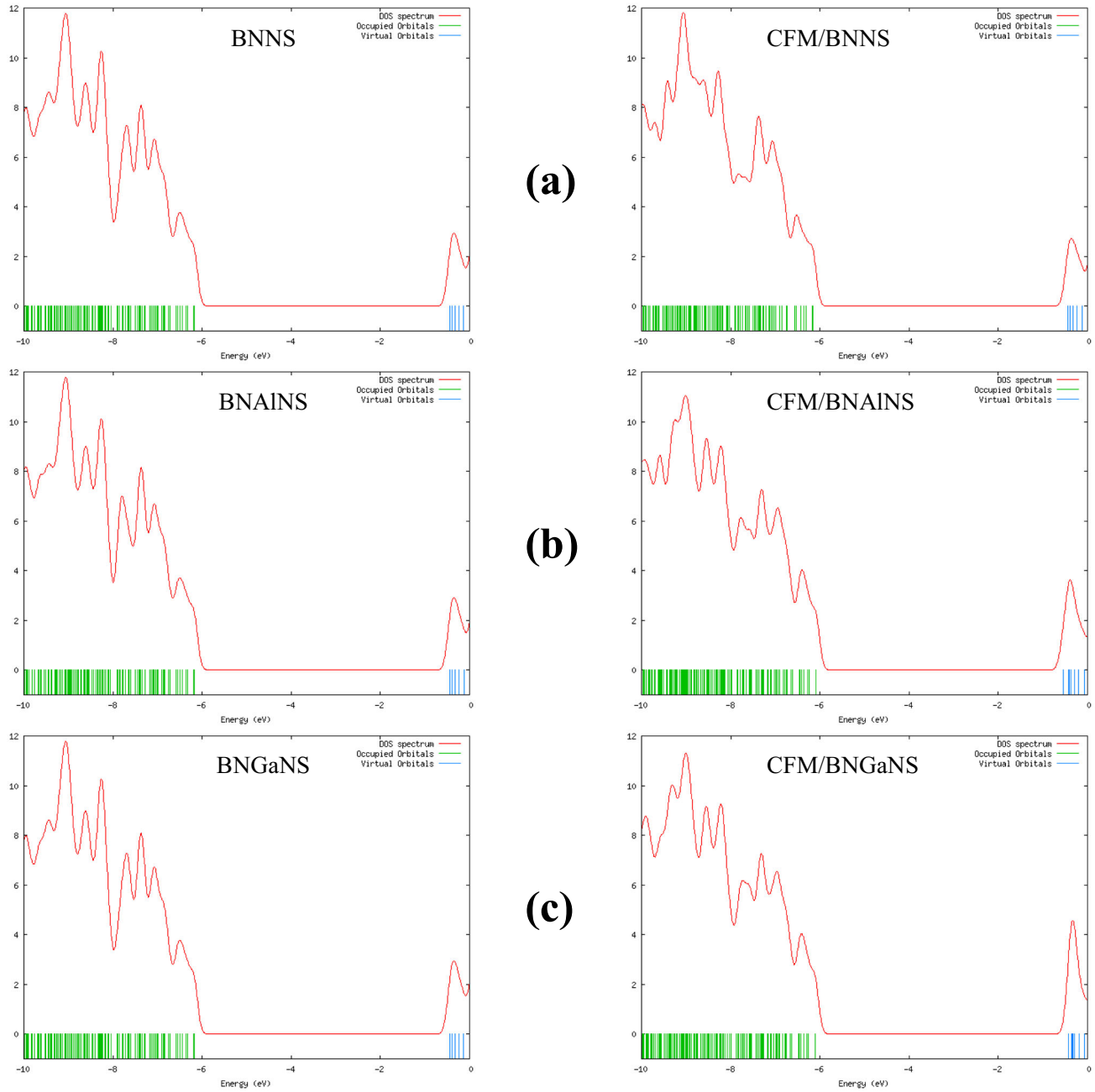


**Fig. 5** The density of state (DOS) diagrams for the adsorption of CFM molecule onto the surface of the **a** pristine, **b** Al-doped, **c** Ga-doped boron nitride nanosheets. The data were obtained from completed nanosheet and B3LYP-D3/6-311G(d) level of theory. The left side diagrams are isolated nanosheets, and the right side diagrams are CFM/nanosheet clusters

rotation barrier, and hydrogen bonding. In NBO analysis, molecular energy is divided into two parts: total energy (for non-stationary enters) and Lewis molecule energy (where super-conjugation does not occur, and the electrons are strongly bound in single bonds and pairs). The occupied NBOs describe the covalent effects in the molecule, while the non-occupied NBOs are used to describe non-covalent effects. The most important non-occupied NBOs are anti-bond orbitals [47, 59, 60].

Various types of bond order analyses are developed to take into account the bond property such as Mulliken bond order analysis [61], Mayer bond order analysis [62, 63], multi-center bond order analysis [64, 65], Wiberg bond order analysis [66], and fuzzy bond order [67, 68]. Due to the different assumptions, caution should be exercised when using the abovementioned methods and the term "Caveat emptor" in this case is a practical example to describe such a situation. Basis set containing diffuse functions as case in point leads to unreliable result for Mulliken or Mayer analyses [33].

According to the literature [69], the Wiberg bond order, in comparison to the Mayer method, has much less sensitivity to the basis set. The Wiberg bond index (WBI) is the sum of squares of off-diagonal density matrix elements between atoms and is denoted as follows:

$$\mathrm{WBI} = \sum_k p_{jk}^2 = 2p_{jj} - p_{jk}^2 \tag{19}$$

where *Pjk* represents the density matrix elements (i.e., the contribution of interactions between basis functions j and k) and *Pjj* is the charge density in the atomic orbital. In the WBI, there is no difference between net bonding or antibonding type of elements of the density matrix.

NBO analysis was used to calculate the bond order using the Wiberg method [66] for a more detailed examination of the types of interactions. After studying the adsorption energy of the complexes, we examine the bond length and bond order of the gases and the nanosheets before and after the adsorption. The Wiberg bond order for these clusters is reported in Table 4. According to this table, that the bond of the halogen atoms in CFM molecules oriented to the N in BNNS, Al in BNAlNS and Ga in GaNNS are the most significant bonds. The results of the WBI analysis agree with the adsorption energies reported in Table 1. They reveal that these nanosheets show a strong interaction with the gas molecules and can be considered a suitable sensor for such gases.

One of the results of the natural population analysis obtained from NBO calculation is a natural electron configuration which shows the effective valence electron configuration for any atoms in the studied structure. The results of the NBO calculations shed light on the natural electron configuration and partial natural charge, which are useful in the study of the character of the bond between the CFM and the nanosheets. The NBO approach was implemented for all atoms in the pristine and cluster systems to reveal the quantities listed in Table 5. Charge transfer quantity between CFM molecule and nanosheets can also be a criteria to study the interaction of nanosheet and CFM, such that the stronger the interaction, the more the charge transfer between CFM and the nanosheet. Table 5 shows that there is a significant charge transfer between two species during adsorption process.

**Table 4** The Wiberg bond index (WBI), obtained for atomic bonds and intermolecular interactions between CFM molecule and BNNS, BNAlNS, and BNGaNS. All calculations were performed using B3LYP-D3/6-311G(d) level of theory

| Systems | F.... (x) | F....B | F....N | C–F | Cl....F | H....F |
|---|---|---|---|---|---|---|
| $CH_2ClF$/BNNS | - | 0.001 | 0.002 | 0.872 | 0.072 | 0.022 |
| $CH_2ClF$/BNAlNS | 0.200 | 0.001 | 0.008 | 0.725 | 0.061 | 0.012 |
| $CH_2ClF$/BNGaNS | 0.188 | 0.001 | 0.010 | 0.756 | 0.063 | 0.014 |

In addition, by implementing the natural electron configuration, the type of the interaction between nanosheets and CFM molecule will be described. From Table 5 it can be obvious that valance configuration of isolated CFM molecule and nanosheets as well as valance configuration of nanosheet/CFM clusters have been increased. Therefore, the interaction of CFM with all nanosheets can be classified as a strong chemisorption process.

The second-order perturbation is an estimation of donor–acceptor interactions in the NBO basis. NBO analysis expresses the complex quantum-mechanical wavefunction into a more palpable Lewis-dot-like formalism. Lewis-type NBOs are called filled or "donor" orbitals ($\sigma$), and non-Lewis-type NBOs are called vacant or "acceptor" orbitals ($\sigma^*$). For each donor NBO ($i$) and acceptor NBO ($j$), the stabilization energy $E(2)$ is calculated as follow [57]:

$$E(2) = \Delta E_{ij}^2 = -q_i \frac{\left(F_{i,j}\right)^2}{\left(\varepsilon_j - \varepsilon_i\right)} \tag{20}$$

where $\varepsilon i$ and $\varepsilon j$ are diagonal elements which show the orbital energies, $q_i$ denotes the donor orbital occupancy ($q = 2$ for closed-shell systems and $q = 1$ for open-shell systems), and the off-diagonal NBO Fock matrix element is demonstrated by *F(i,j)*, and $\Delta E_{ij}^2$ is the stabilization energy.

The results of electron donor–acceptor electron configuration of pristine BNNS and doped BN (Al), and BN (Ga) nanosheets are reported in Table 6. It is noteworthy that in this table the most important interactions in terms of the electron transfer stability energy are reported. The existence of such interactions with the remarkable stability energies in this table shows that in all cases the doped atom has been incorporated into the nanosheet structure by the chemical interaction and the stability structure has been achieved. In other words, the inserted atom behaves as a doping atom. The data in Table 6 show that the most important interaction for the pristine nanosheet related to electron transfer from the BD (B–N) bond as the electron donor to the BD*(C–F) as the receptor. This is in agreement with the results of the absorption energy as well as with the other results which have been examined. In the study of the doped complexes, it is observed that in the Al-complex, the Al electron pair is the Al receptor (Lewis acid) and the N-bonded electron pair is the amino group of the electron donor molecule (Lewis base). The highest electron–acceptor stabilization energy in all cases is due to the same interaction, which indicates a strong adsorption of the molecule onto the BN (Al) nanosheet compared with the others.

## QTAIM analysis

QTAIM is a powerful tool for topology analysis containing the type and structure of bonds and intermolecular

**Table 5** Natural electron configurations and natural charges (au) for the isolated CFM, pristine and Al- and Ga-doped nanosheets and their complex structures. All values calculated by the PBEPBE/6-311G(d) level of theory

| Systems | Atom | Natural charge | Natural electron configuration |
|---|---|---|---|
| BNNS | B | 1.18 | [core]2S(0.63)2p(1.52)3p(0.01)3d(0.01) |
| | N | − 1.18 | [core]2S(1.35)2p(4.82) |
| BNAlNS | B | 1.18 | [core]2S(0.63)2p(1.52)3p(0.01)3d(0.01) |
| | N | − 1.18 | [core]2S(1.37)2p(4.75) |
| | Al | 2.01 | [core]3S(0.40)3p(0.58)3d(0.02) |
| BNGaNS | B | 1.18 | [core]2S(0.63)2p(1.52)3p(0.01)3d(0.01) |
| | N | − 1.18 | [core]2S(1.37)2p(4.75) |
| | Ga | 1.80 | [core]4S(0.56)4p(0.66)4d(0.01) |
| $CH_2ClF$/BNNS | B | 1.18 | [core]2S(0.63)2p(1.52)3p(0.01)3d(0.01) |
| | N | − 1.18 | [core]2S(1.37)2p(4.75) |
| | C | 0.01 | [core]2S(1.12)2p(2.85)3p(0.01)3d(0.01) |
| | H | 0.22 | 1S(0.78) |
| | Cl | − 0.08 | [core]3S(1.87)3p(5.19)3d(0.01)4p(0.01) |
| | F | − 0.35 | [core]2S(1.85)2p(5.50) |
| $CH_2ClF$/BNAlNS | B | 1.18 | [core]2S(0.63)2p(1.52)3p(0.01)3d(0.01) |
| | N | − 1.18 | [core]2S(1.37)2p(4.75) |
| | Al | 2.03 | [core]3S(0.40)3p(0.54)3d(0.02)4p(0.01) |
| | C | − 0.05 | [core]2S(1.16)2p(2.87)3p(0.01)3d(0.01) |
| | H | 0.26 | 1S(0.74) |
| | Cl | 0.02 | [core]3S(1.86)3p(5.10)3d(0.01)4p(0.01) |
| | F | − 0.37 | [core]2S(1.84)2p(5.52) |
| $CH_2ClF$/BNGaNS | B | 1.18 | [core]2S(0.63)2p(1.52)3p(0.01)3d(0.01) |
| | N | − 1.18 | [core]2S(1.38)2p(4.74) |
| | Ga | 1.82 | [core]4S(0.56)4p(0.62)5p(0.01) |
| | C | − 0.04 | [core]2S(1.15)2p(2.88)3p(0.01)3d(0.01) |
| | H | 0.25 | 1S(0.75) |
| | Cl | 0.01 | [core]3S(1.86)3p(5.12)3d(0.01)4p(0.01) |
| | F | − 0.35 | [core]2S(1.84)2p(5.50) |
| $CH_2ClF$ | C | − 0.04 | [core]2S(1.13)2p(2.89)3p(0.01)3d(0.01) |
| | H | 0.22 | 1S(0.77) |
| | Cl | − 0.32 | [core]3S(1.88)3p(5.19)3d(0.01)4p(0.01) |
| | F | − 0.08 | [core]2S(1.84)2p(5.47) |

interactions. QTAIM method was proposed by Bader et al. [70–75]. According to this theory, the critical point of the electron density, which can be a minimum point, a maximum point, or a saddle point, can fall into one of the following four categories: (1) *atomic critical point* (ACP), which denotes the geometrical position of an atom or nucleus (other than hydrogen), and geometrically represents a local maximum point of electron density in all three directions of space; (2) *bond critical point* (BCP), which indicates a critical point related to a bond or physical or chemical interaction (in reality, this point represents a saddle point with two directions of maximum electron density and one direction of minimum electron density); (3) *ring critical point* (RCP) [76, 77], which denotes a ring or set of atoms forming a ring (geometrically, it is a saddle point with the minimum electron density in one direction and in the other two directions); and (4) *cage critical point* (CCP), which is observed when multiple rings form a cage (geometrically, this point is a local minimum point in all three directions of space). Poincaré–Hopf relationship should be satisfied to verify if all CPs may have been found as follows [78, 79]:

$$n_{(ACP)} - n_{(BCP)} + n_{(RCP)} - n_{(CCP)} = 1 \quad (21)$$

The eigenvalues of Hessian matrix, $\lambda_1$ and $\lambda_2$, are negative and $|\lambda_1| < |\lambda_2|$ for the BCP. $\lambda_1$ and $\lambda_2$ are perpendicular to the bonding path, and $\lambda_3$ is a positive value along the bonding path. For the QTAIM analysis, is it necessary to know the electron density $\rho(r)$ and Laplacian electron density $\nabla^2 \rho(r)$. The $\rho(r)$ and $\nabla^2\rho(r)$ play an important role in the segmentation and identification of different types of chemical interactions.

**Table 6** The donor–acceptor NBO interactions and second-order perturbation energies ($E(2)$) for the CFM clusters with BNNS, BNAlNS, and BNGaNS. All values obtained from completed nanosheets at the PBEPBE/6-311G(d) level of theory

| Systems | Donor NBO (i) | Acceptor NBO (j) | E(2) (kcal/mol) |
|---|---|---|---|
| $CH_2ClF$/BNNS | BD (B-N) | BD*(C–H) | 0.07 |
| | BD (B-N) | BD*(C–F) | 0.13 |
| $CH_2ClF$/BNAlNS | BD (B-N) | LP*(Al) | 14.8 |
| | BD (B-N) | RY*(Al) | 0.74 |
| | BD (B-N) | BD*(C–Cl) | 0.05 |
| | BD (B-N) | BD*(C–H) | 0.09 |
| | BD (B-N) | BD*(C–F) | 1.18 |
| $CH_2ClF$/BNGaNS | BD (N-Ga) | BD*(C–F) | 0.73 |
| | BD (B-N) | BD*(C–H) | 0.07 |
| | BD (B-N) | BD*(C–F) | 0.54 |
| | BD (B-N) | RY*(F) | 0.13 |
| | BD (B-N) | RY*(Cl) | 0.07 |

A BCP with negative values of $\nabla^2\rho(r)$ and large values of $\rho(r)$ (of orders exceeding 10–1 a.u.) is defined as a shared (covalent) intermolecular interaction. Also, when $\nabla^2\rho(r)$ is positive, the interactions can be classified as of the non-substrate close-shell type (which include ionic and van der Waals interactions) [80]. The elliptical bond (ε) [81] and the virial theorem [82] are two other important factors in the classification of bonds. An elliptical bond represents the electron density preferentially accumulated on a plate containing the bond and is defined as follows:

$$\varepsilon = \frac{\lambda_1}{\lambda_2} - 1 \quad \text{where } |\lambda_1| > |\lambda_2| \tag{22}$$

Large values of ε indicate an unstable structure and vice versa. Also, based on the virial theorem, the following relationship exists between the electron kinetic energy density $G(r)$ [83], the electron potential energy density $V(r)$ [84], and $\nabla^2\rho(r)$:

**Table 7** The AIM topological parameters, including electron density ($\rho(r)$), Laplacian of electron density ($\nabla^2\rho(r)$), the kinetic electron density $G(r)$, potential electron density $V(r)$, eigenvalues of Hessian matrix ($\lambda$), and bond ellipticity index ($\varepsilon$) at BCPs of the CFM clusters with BNNS, BNAlNS, BNGaNS. All values have been calculated using the B3LYP-D3/6-311G(d) level of theory from NBO analysis

| Systems | Bond | $\rho$ | $\nabla^2 r$ | $G(r)$ | $V(r)$ | $G(r)/V(r)$ | $\lambda_1$ | $\lambda_2$ | $\lambda_3$ | $\varepsilon$ |
|---|---|---|---|---|---|---|---|---|---|---|
| CH2ClF | C–H | 0.2788 | − 0.9946 | 0.0287 | − 0.3061 | 0.0939 | − 0.7828 | − 0.7617 | 0.5499 | 0.0277 |
| | C–Cl | 0.1765 | − 0.1940 | 0.0597 | − 0.1680 | 0.3557 | − 0.2799 | − 0.2657 | 0.3517 | 0.0532 |
| | C–F | 0.2550 | − 0.1198 | 0.3286 | − 0.6872 | 0.4782 | − 0.4988 | − 0.4292 | 0.8082 | 0.1621 |
| BNNS | B–N | 0.1923 | 0.4258 | 0.2717 | − 0.4370 | 0.6218 | − 0.4516 | − 0.4440 | 1.3215 | 0.0171 |
| BNAlNS | Al–N | 0.1137 | 0.8632 | 0.2269 | − 0.2380 | 0.9534 | − 0.2090 | − 0.1848 | 1.2571 | 0.1309 |
| BNGaNS | Ga–N | 0.1533 | 0.7746 | 0.2501 | − 0.3066 | 0.8158 | − 0.2317 | − 0.2230 | 1.2294 | 0.0389 |
| $CH_2ClF$/BNNS | F....N | 0.0067 | 0.0276 | 0.0057 | − 0.0046 | 1.2553 | − 0.0049 | − 0.0016 | 0.0342 | 1.9883 |
| | C....N | 0.0042 | 0.0154 | 0.0030 | − 0.0021 | 1.4129 | − 0.0025 | − 0.0012 | 0.0191 | 1.1781 |
| | B–N | 0.0142 | 0.0535 | 0.0113 | − 0.0093 | 1.2180 | − 0.0160 | − 0.0112 | 0.0806 | 0.4270 |
| | C–H | 0.2836 | − 1.0464 | 0.0264 | − 0.3145 | 0.0841 | − 0.8105 | − 0.7885 | 0.5526 | 0.0280 |
| | C–Cl | 0.2489 | − 0.0817 | 0.3292 | − 0.6788 | 0.4850 | − 0.4939 | − 0.4134 | 0.8256 | 0.1948 |
| | C–F | 0.2823 | − 1.0316 | 0.0270 | − 0.3120 | 0.0867 | − 0.8028 | − 0.7801 | 0.5513 | 0.0290 |
| $CH_2ClF$/BNAlNS | F....Al | 0.0345 | 0.2035 | 0.0494 | − 0.0479 | 1.0310 | − 0.0433 | − 0.0424 | 0.2892 | 0.0228 |
| | C....N | 0.0117 | 0.0361 | 0.0080 | − 0.0070 | 1.1412 | − 0.0107 | − 0.0070 | 0.0538 | 0.5237 |
| | Al–N | 0.1002 | 0.7011 | 0.1831 | − 0.1910 | 0.9590 | − 0.1735 | − 0.1594 | 1.0340 | 0.0882 |
| | B–N | 0.1960 | 0.4614 | 0.2841 | − 0.4529 | 0.6274 | − 0.4641 | − 0.4485 | 1.3741 | 0.0348 |
| | C–H | 0.2859 | − 1.0849 | 0.0248 | − 0.3207 | 0.0772 | − 0.8288 | − 0.8038 | 0.5476 | 0.0311 |
| | C–Cl | 0.2020 | − 0.2983 | 0.0649 | − 0.2044 | 0.3176 | − 0.3349 | − 0.3197 | 0.3563 | 0.0473 |
| | C–F | 0.1941 | − 0.1077 | 0.2047 | − 0.4363 | 0.4691 | − 0.3003 | − 0.2359 | 0.4285 | 0.2731 |
| $CH_2ClF$/BNGaNS | F....Ga | 0.0479 | 0.2047 | 0.0596 | − 0.0681 | 0.8757 | − 0.0559 | − 0.0543 | 0.3150 | 0.0295 |
| | C...N | 0.0099 | 0.0312 | 0.0068 | − 0.0058 | 1.1666 | − 0.0086 | − 0.0047 | 0.0445 | 0.8147 |
| | Ga–N | 0.1327 | 0.6356 | 0.2016 | − 0.2444 | 0.8251 | − 0.1893 | − 0.1828 | 1.0077 | 0.0354 |
| | B–N | 0.1963 | 0.4824 | 0.2881 | − 0.4556 | 0.6324 | − 0.4663 | − 0.4506 | 1.3993 | 0.0347 |
| | C–H | 0.2855 | − 1.0772 | 0.0252 | − 0.3197 | 0.0788 | − 0.8247 | − 0.8002 | 0.5477 | 0.0305 |
| | C–Cl | 0.1973 | − 0.2817 | 0.0633 | − 0.1970 | 0.3212 | − 0.3263 | − 0.3105 | 0.3551 | 0.0510 |
| | C–F | 0.2069 | − 0.1074 | 0.2345 | − 0.4958 | 0.4729 | − 0.3391 | − 0.2691 | 0.5008 | 0.2600 |

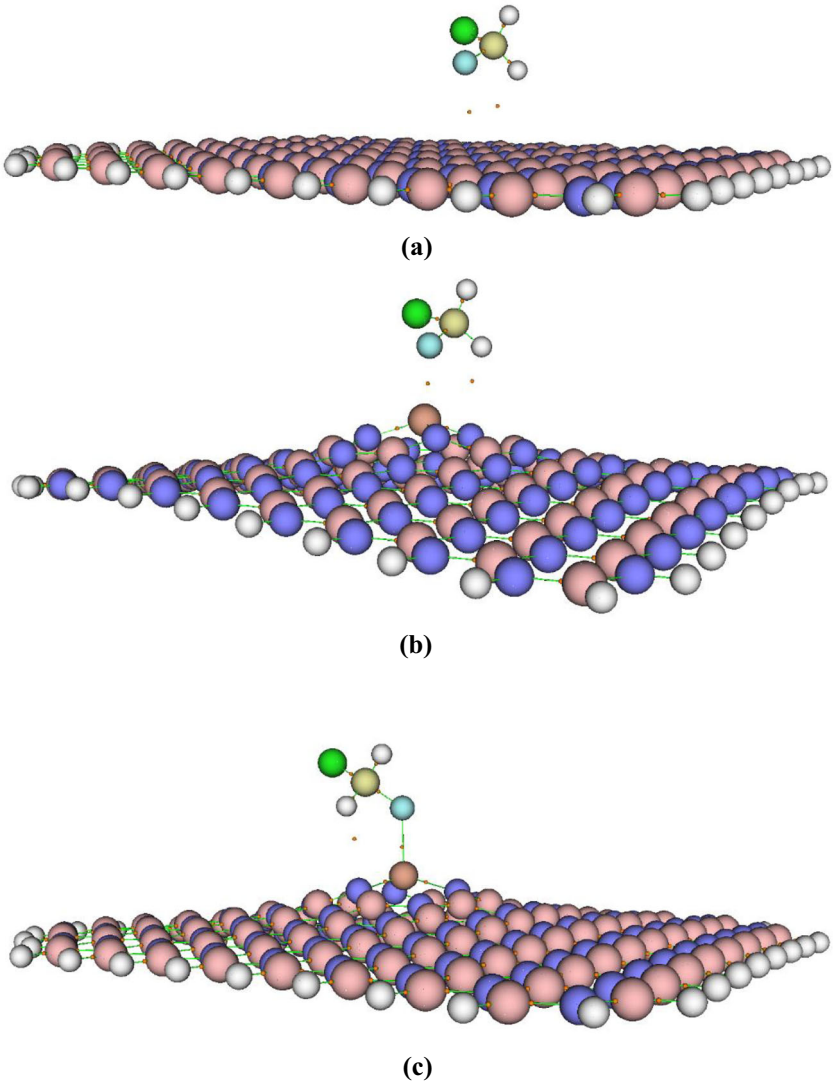


**Fig. 6** AIM molecular graphs for **a** CFM/BNNS, **b** CFM/BNAlNS, and **c** CFM/BNGaNS systems. Orange dots represent the boundary critical points (BCPs)

$$\frac{1}{4}\nabla^2\rho(r) = 2G(r) + V(r) \tag{23}$$

The balance between $G(r)$ and $V(r)$ reflects the nature of the interaction, and therefore, the ratio of $G/|V|$ can be used as an appropriate index in link classification. If this ratio is less than 0.5, the nature of the interaction will be purely covalent, and if the ratio is greater than 1, the interaction may be considered completely non-covalent. Note that for covalent bonds (i.e., $\nabla^2\rho(r) < 0$ and $G/|V| < 0.5$), the nature of the bond changes from van der Waals interactions to strong covalent interactions. It becomes covalent. It can also play a decisive role in controlling the amount of ionic interaction for close-shell interactions (i.e., $\nabla^2\rho(r) > 0$ and $G/|V| > 1$), as they become stronger ionically (and weakly electrostatic) by reducing interactions. Therefore, the QTAIM topology analysis together with WBI analysis and adsorption results expose an important trend: by increasing the ionic character of atomic bonds in the nanosheets, the tendencies of the gases to adsorb are also increased.

Considerable results can be obtained from reviewing Table 7. It is observed that in all adsorption sites Laplacin of electron energy density has a positive value; that is, the bond is noncovalent. In the study of doped systems, we found that for the all clusters the energy density and the energy density of Laplacin are high indicating that there is a strong bond between the nanosheets and the CFM molecule and the elliptical bond is close to 0, which means the interaction is strong. As stated above, when the ratio of $G/|V|$ is more than 1, it means non-covalent bonding, in the case of Ga-doped clusters these amounts are less than 1. In other words, the results of QTAIM analysis also confirm the strong adsorption of the CFM molecule on the BN(Al)NT and BN(Ga)NT (Fig. 6).

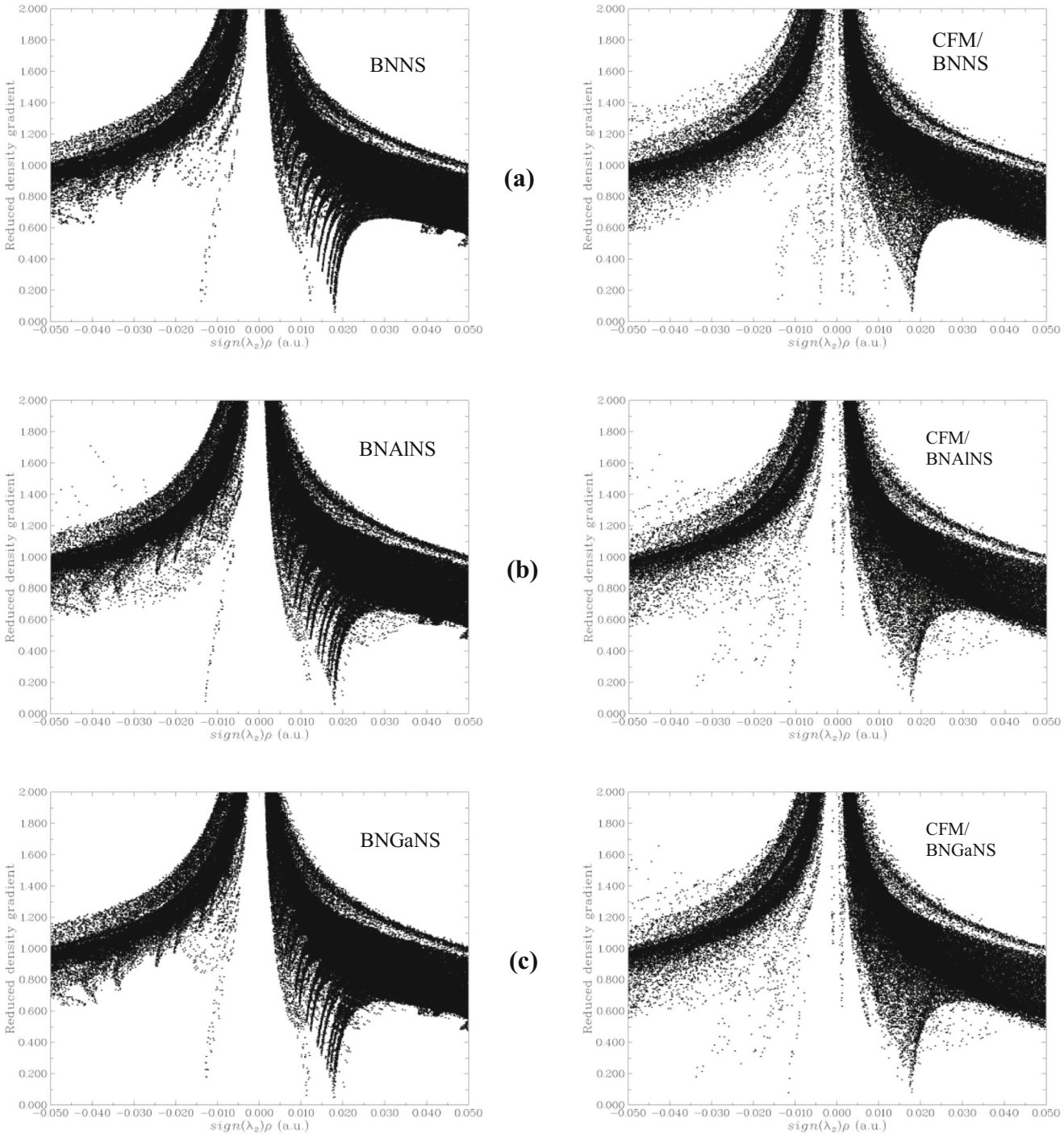


**Fig. 7** Plots for the reduced density gradient (RDG) vs. sign($\lambda_2$)$\rho$(r) values of the **a** pristine **b** Al-doped, and **c** Ga-doped boron nitride nanosheets. The data were obtained from completed nanosheet and B3LYP-D3 /6-311G(d) level of theory. The left side diagrams are isolated nanosheets and the right side diagrams are CFM/nanosheet clusters

The reduced density gradient (RDG) function and sign$\lambda_2$(r)$\rho$(r) are used to evaluate the weak interactions. These functions are categorized in the context of non-covalent interaction methods which is powerful way to analyze the types of intermolecular interactions. The RGD is defined as follows [85, 86]:

$$\mathrm{RDGs} = \frac{1}{2(3\pi^2)^{\frac{1}{3}}} \frac{\left|\overline{\Delta\rho}(r)\right|}{\overline{\rho(r)}^{\frac{4}{3}}} \tag{24}$$

The strength of the interaction has a positive correlation with electron density $\rho$(r) and the second largest eigenvalue

of the Hessian matrix ($\lambda_2$). Thus, the real space function $\text{sign}\lambda_2(r)\rho(r)$ (the products of the signs of $\lambda_2$ and $\rho$) can be defined. The scatter graph of the sign of the $\lambda_2(r)\rho(r)$ function (X-axis) and RDG (Y-axis) reveals the interaction type between gases and nanosheets. The RDG values range from medium to very large around the nuclei and edges of the molecules, whereas weak interactions (zero to medium) are observed around the chemical bonds. Also, for each specific value of RDG (seen as a horizontal line on the graph), the regions of the graph can be classified into three types, namely, $\text{sign}\lambda_2(r)\rho(r) < 0$ (strong attraction), $\text{sign}\lambda_2(r)\rho(r) \approx 0$ (weak van der Waals interaction), and $\text{sign}\lambda_2(r)\rho(r) > 0$ (strong repulsion (steric effect in ring)) [85, 86].

Using the isosurface RDG = 0.5 as a reference, it can be concluded that after adsorption of the gas onto the outer surfaces of the nanosheets, spots appeared around the region characterized by $\text{sign}\lambda_2(r)\rho(r) \approx 0$. The interaction of gas with BN nanosheets is in the range of strong van der Waals interactions in nature. Significant changes in the overall features of the pristine nanosheet graph (Fig. 7) after the adsorption of gases were observed in the region characterized as $\text{sign}\lambda_2(r)\rho(r) < 0$ (i.e., strong attraction), implying that the nanosheet/gas interactions were strong. Hence, this analysis also confirms the results of the single-point energy calculations and NBO analysis, namely that the interactions of CFM with BNNS, BNAlNS, and BNGaNS were strong.

## Conclusions

In this study, the interactions between chlorofluoromethane molecule and pristine, and Al- and Ga-doped boron nitride nanosheets were investigated using density functional framework. To this end, the structure of the nanosheets and CFM molecule was optimized at the theoretical level of PBE-PBE/6-311G (d). Right after that, B3LYP-D3, M062X, and wB97XD functionals and same basis set were also used to consider the contribution of long-range interactions and dispersion effect. QTAIM and NBO analyses were also implemented to consider the character of intermolecular interactions. The results of all analyses are in agreement and show the following: (1) among the different positions studied for pristine boron nitride nanosheet, the $T_3$ position has the highest absorption energy; (2) investigations in this study show that the Al and Ga elements can be substituted by BNNS nanosheet atoms by chemical bonding and, as a binding element, cause dramatic changes in the chemical, electronic, and mechanical structure of BNNS nanosheets; (3) among the doped nanosheets, Ga-doped BNNS has a very high adsorption energy compared with other elements, and is expected to be chemically adsorbed in this case and appears to be a suitable sensor characteristic option. The next category is Al element, where the adsorption energy is higher than the initial state but lower than that of Ga. Generally, we found that the adsorption tendencies of the aforementioned gas molecule have a positive correlation to the nature of the bonds in BN nanosheets. Finally, we, according to the results obtained from energy gap and adsorption energies, conclude that the BNNS, BNAlNS, and BNGaNS are favorable candidates for utilization as gas sensor devices to detect CFM molecule.

**Acknowledgments** The authors would like to thank the Solid-State Theory Group at the Physics Department at the Universita'degli Studi di Milano-Italy for providing computational facilities.

## Compliance with ethical standards

**Conflict of interest** The authors declare that they have no conflict of interest.

## References

1. Abbasi M, Nemati-Kande E, Mohammadi MD (2018) Doping of the first row transition metals onto B12N12 nanocage: a DFT study. Comput Theoretical Chem 1132:1–11
2. Ahmadi R (2012) Computational study of chemical properties of captopril drug and the connected form to fullerene (C60) as a medicine nano carrier. J Phys Theor Chem 9:185–190
3. Ahmadi R, Salmaniha M (2014) Investigation of chemical properties in fullerene derivatives of fluoxetine drug: a DFT study. Int J New Chem 1:151–159
4. Esrafili MD, Mousavian P, Rad FA (2018) Adsorption of formamide over pristine and Al-doped boron nitride nanosheets: a dispersion-corrected DFT study. J Mol Graph Model 82:101–107
5. Mohammadi MD, Hamzehloo M (2018) The adsorption of bromomethane onto the exterior surface of aluminum nitride, boron nitride, carbon, and silicon carbide nanotubes: a PBC-DFT, NBO, and QTAIM study. Comput Theoretical Chem 1144:26–37
6. Nemati-Kande E, Abbasi M, Doust Mohammadi M (2018) DFT, QTAIM and NBO investigation of the interaction of rare gases with pristine and decorated boron nitride nanotube. ChemistrySelect 3:9833–9840
7. Nemati-Kande E, Abbasi M, Mohammadi MD (2020) DFT studies on the interactions of pristine, Al and Ga-doped boron nitride nanosheets with CH3X (X= F, Cl and Br). J Mol Struct 1199:126962
8. Nemati-Kande E, Abbasi M, Mohammadi MD (2019) Feasibility of pristine and decorated AlN and SiC nanotubes in sensing of noble gases: a DFT study. ChemistrySelect 4:2453–2462
9. Nemati-Kande E, Karimian R, Goodarzi V, Ghazizadeh E (2020) Feasibility of pristine, Al-doped and Ga-doped boron nitride nanotubes for detecting SF4 gas: a DFT, NBO and QTAIM Investigation. Appl Surf Sci:145490
10. Li LH, Xing T, Chen Y, Jones R (2014) Boron nitride nanosheets for metal protection. Adv Mater Interfaces 1:1300132
11. Fu L, Chen G, Jiang N, Yu J, Lin C-T, Yu A (2016) In situ growth of metal nanoparticles on boron nitride nanosheets as highly efficient catalysts. J Mater Chem A 4:19107–19115
12. Luo W, Wang Y, Hitz E, Lin Y, Yang B, Hu L (2017) Solution processed boron nitride nanosheets: synthesis, assemblies and emerging applications. Adv Funct Mater 27:1701450
13. Raza MA, Nadeem A, Ilyas MT (2019) Corrosion study of boron nitride nanosheets deposited on copper metal by electrophoretic deposition. TMS 2019 148th Annual Meeting & Exhibition Supplemental Proceedings. Springer, pp 681–685

14. Omidirad R, Azizi K (2019) DFT study of charge-controlled mechanism of water molecule dissociation on vacancy defected boron nitride nanosheets. J Mol Graph Model 93:107448
15. Esrafili MD, Saeidi N (2018) Carbon-doped boron nitride nanosheet as a promising catalyst for N2O reduction by CO or SO2 molecule: a comparative DFT study. Appl Surf Sci 444:584–589
16. Esrafili MD (2018) NO reduction by CO molecule over Si-doped boron nitride nanosheet: a dispersion-corrected DFT study. Chem Phys Lett 695:131–137
17. Moladoust R, Esrafili MD, Hosseinian A, Alkorta I, Vessally E (2019) Adsorption sensitivity of pristine and Al-or Si-doped boron nitride nanoflake to COCl2: a DFT study. Mol Phys 117:626–634
18. Esrafili MD (2018) Epoxidation of ethylene over carbon and silicon-doped boron nitride sheets: a comparative DFT study. Solid State Commun 284:35–39
19. Esrafili MD, Asadollahi S, Heydari S (2019) A DFT study on NO reduction to N2O using Al-and P-doped hexagonal boron nitride nanosheets. J Mol Graph Model 89:41–49
20. Dorn RW, Ryan MJ, Kim T-H, Goh TW, Venkatesh A, Heintz PM, Zhou L, Huang W, Rossini AJ (2020) Identifying the molecular edge termination of exfoliated hexagonal boron nitride Nanosheets with solid-state NMR spectroscopy and plane-wave DFT calculations. Chem Mater 32:3109–3121
21. Ai Z, Chang B, Xu C, Huang B, Wu Y, Hao X, Shao Y (2019) Interface engineering in the BNNS@ Ti 3 C 2 intercalation structure for enhanced electrocatalytic hydrogen evolution. New J Chem 43:8613–8619
22. Azamat J, Khataee A, Joo SW (2016) Separation of copper and mercury as heavy metals from aqueous solution using functionalized boron nitride nanosheets: a theoretical study. J Mol Struct 1108:144–149
23. Esrafili MD, Saeidi N (2017) A DFT study on the healing of N-vacancy defects in boron nitride nanosheets and nanotubes by a methylene molecule. Int J Quantum Chem 117:e25450
24. Esrafili MD, Saeidi N, Nematollahi P (2016) The healing of B-or N-vacancy defective BNNTs by using CO molecule: a DFT study. New J Chem 40:8024–8031
25. Li H, Chen Z, Fang X, Tie D (2015) Absorption of NH3 on pristine and defected boron nitride nanosheets: a first principle study. Superlattice Microst 88:371–376
26. Lin S, Huang J, Gao X (2015) A Cu (111) supported h-BN nanosheet: a potential low-cost and high-performance catalyst for CO oxidation. Phys Chem Chem Phys 17:22097–22105
27. Binbrek OS, Torrie BH, Swainson IP (2002) Neutron powder-profile study of chlorofluoromethane. Acta Crystallogr Sect C: Cryst Struct Commun 58:o672–o674
28. U.N.E.P.O. Secretariat, Handbook for the Montreal protocol on substances that deplete the ozone layer, UNEP/Earthprint2006
29. Favero LB, Maris A, Melandri S, Ottaviani P, Caminati W (2019) Non covalent interactions stabilizing the chiral dimer of CH 2 ClF: a rotational study. Phys Chem Chem Phys 21:3695–3700
30. Perdew JP, Burke K, Ernzerhof M (1996) Generalized gradient approximation made simple. Phys Rev Lett 77:3865
31. Hehre WJ, Ditchfield R, Pople JA (1972) Self—consistent molecular orbital methods. XII. Further extensions of Gaussian—type basis sets for use in molecular orbital studies of organic molecules. J Chem Phys 56:2257–2261
32. Frisch M, Trucks G, Schlegel H, Scuseria G, Robb M, Cheeseman J, Scalmani G, Barone V, Petersson G, Nakatsuji H (2016) Gaussian 16. Gaussian, Inc., Wallingford CT **(2016)**
33. Lu T, Chen F (2012) Multiwfn: a multifunctional wavefunction analyzer. J Comput Chem 33:580–592
34. Lu T, Chen F (2012) Quantitative analysis of molecular surface based on improved Marching Tetrahedra algorithm. J Mol Graph Model 38:314–323
35. Lu T, Chen Q (2020) A simple method of identifying π orbitals for non-planar systems and a protocol of studying π electronic structure. Theor Chem Accounts 139:25
36. J.B. Foresman, A. Frisch, Exploring chemistry with electronic structure methods: a guide to using Gaussian, (1996)
37. Grimme S (2006) Semiempirical GGA-type density functional constructed with a long-range dispersion correction. J Comput Chem 27:1787–1799
38. Grimme S, Antony J, Ehrlich S, Krieg H (2010) A consistent and accurate ab initio parametrization of density functional dispersion correction (DFT-D) for the 94 elements H-Pu. J Chem Phys 132: 154104
39. Grimme S, Ehrlich S, Goerigk L (2011) Effect of the damping function in dispersion corrected density functional theory. J Comput Chem 32:1456–1465
40. Parr RG, Donnelly RA, Levy M, Palke WE (1978) Electronegativity: the density functional viewpoint. J Chem Phys 68:3801–3807
41. von Szentpály L (1998) Valence states in molecules. 3. Transferable vibrational force constants from homonuclear data. J Phys Chem A 102:10912–10915
42. Janak J (1978) Proof that∂ e∂ n i= ε in density-functional theory. Phys Rev B 18:7165
43. Parr RG (1980) Density functional theory of atoms and molecules. Horizons of Quantum Chemistry, Springer, Berlin
44. Chattaraj P, Perennial RD, Parr RG (1991) HSAB principle. J Am Chem Soc 113:1855–1856
45. Parr RG (1922-1924) L.v. Szentpaly, S. Liu, Electrophilicity index. J Am Chem Soc 121(1999)
46. Noorizadeh S, Maihami H (2006) A theoretical study on the regioselectivity of Diels–Alder reactions using electrophilicity index. J Mol Struct THEOCHEM 763:133–144
47. Weinhold F (2012) Discovering chemistry with natural bond orbitals. John Wiley & Sons, New York
48. Weinhold F, Landis CR (2005) Valency and bonding: a natural bond orbital donor-acceptor perspective. Cambridge University Press, Cambridge
49. Carpenter J, Weinhold F (1988) Analysis of the geometry of the hydroxymethyl radical by the "different hybrids for different spins" natural bond orbital procedure. J Mol Struct THEOCHEM 169:41–62
50. Foster AJ, Weinhold F (1980) Natural hybrid orbitals. J Am Chem Soc 102:7211–7218
51. Glendening E, Badenhoop J, Reed A, Carpenter J, Bohmann J, Morales C, Landis C, Weinhold F (2013) NBO 6.0. Theoretical Chemistry Institute, University of Wisconsin, Madison
52. Reed AE, Weinhold F (1983) Natural bond orbital analysis of near-Hartree–Fock water dimer. J Chem Phys 78:4066–4073
53. Reed AE, Weinhold F (1985) Natural localized molecular orbitals. J Chem Phys 83:1736–1740
54. Reed AE, Weinstock RB, Weinhold F (1985) Natural population analysis. J Chem Phys 83:735–746
55. Glendening ED, Landis CR, Weinhold F (2012) Natural bond orbital methods. Interdiscip Rev Comput Mol Sci 2:1–42
56. Glendening ED, Landis CR, Weinhold F (2019) NBO 7.0: new vistas in localized and delocalized chemical bonding theory. J Comput Chem 40:2234–2241
57. Reed AE, Curtiss LA, Weinhold F (1988) Intermolecular interactions from a natural bond orbital, donor-acceptor viewpoint. Chem Rev 88:899–926
58. Weinhold F (2002) Natural bond orbital methods, encyclopedia of computational chemistry, 3. Hoboken, New Jersey
59. Weinhold F (2012) Natural bond orbital analysis: a critical overview of relationships to alternative bonding perspectives. J Comput Chem 33:2363–2379

60. Weinhold F, Landis C, Glendening E (2016) What is NBO analysis and how is it useful? Int Rev Phys Chem 35:399–440
61. Mulliken RS (1955) Electronic population analysis on LCAO–MO molecular wave functions. I. J Chem Phys 23:1833–1840
62. Mayer I (1983) Charge, bond order and valence in the AB initio SCF theory. Chem Phys Lett 97:270–274
63. Mayer I (2012) Improved definition of bond orders for correlated wave functions. Chem Phys Lett 544:83–86
64. Giambiagi M, de Giambiagi MS, Mundim KC (1990) Definition of a multicenter bond index. Struct Chem 1:423–427
65. Matito E (2016) An electronic aromaticity index for large rings. Phys Chem Chem Phys 18:11839–11846
66. Wiberg KB (1968) Application of the pople-santry-segal CNDO method to the cyclopropylcarbinyl and cyclobutyl cation and to bicyclobutane. Tetrahedron 24:1083–1096
67. Lu T, Chen F (2013) Bond order analysis based on the Laplacian of electron density in fuzzy overlap space. J Phys Chem A 117:3100–3108
68. Mayer I, Salvador P (2004) Overlap populations, bond orders and valences for 'fuzzy'atoms. Chem Phys Lett 383:368–375
69. Sizova OV, Skripnikov LV, Sokolov AY (2008) Symmetry decomposition of quantum chemical bond orders. J Mol Struct THEOCHEM 870:1–9
70. Bader R, Nguyen-Dang TT, Tal Y (1981) A topological theory of molecular structure. Rep Prog Phys 44:893
71. Bader RF (1985) Atoms in molecules. Acc Chem Res 18:9–15
72. Bader RF (1991) A quantum theory of molecular structure and its applications. Chem Rev 91:893–928
73. Bader RF, Matta CF (2013) Atoms in molecules as non-overlapping, bounded, space-filling open quantum systems. Found Chem 15:253–276
74. Biegler-könig FW, Bader RF, Tang TH (1982) Calculation of the average properties of atoms in molecules. II. J Comput Chem 3:317–328
75. Cortés-Guzmán F, Bader RF (2005) Complementarity of QTAIM and MO theory in the study of bonding in donor–acceptor complexes. Coord Chem Rev 249:633–662
76. Howard S, Krygowski T (1997) Benzenoid hydrocarbon aromaticity in terms of charge density descriptors. Can J Chem 75:1174–1181
77. Noorizadeh S, Shakerzadeh E (2010) Shannon entropy as a new measure of aromaticity, Shannon aromaticity. Phys Chem Chem Phys 12:4742–4749
78. Balanarayan P, Gadre SR (2003) Topography of molecular scalar fields. I. Algorithm and Poincaré–Hopf relation. J Chem Phys 119:5037–5043
79. Roy D, Balanarayan P, Gadre SR (2008) An appraisal of Poincaré–Hopf relation and application to topography of molecular electrostatic potentials. J Chem Phys 129:174103
80. Matta CF (2006) Hydrogen–hydrogen bonding: the non-electrostatic limit of closed-shell interaction between two hydro, hydrogen bonding—new insights. Springer, Berlin
81. Bohórquez HJ, Boyd RJ, Matta CF (2011) Molecular model with quantum mechanical bonding information. J Phys Chem A 115:12991–12997
82. Grabowski SJ (2012) QTAIM characteristics of halogen bond and related interactions. J Phys Chem A 116:1838–1845
83. Tal Y, Bader R (1978) Studies of the energy density functional approach. I. Kinetic energy. Int J Quantum Chem 14:153–168
84. Keith T, Bader R, Aray Y (1996) Structural homeomorphism between the electron density and the virial field. Int J Quantum Chem 57:183–198
85. Contreras-García J, Johnson ER, Keinan S, Chaudret R, Piquemal J-P, Beratan DN, Yang W (2011) NCIPLOT: a program for plotting noncovalent interaction regions. J Chem Theory Comput 7:625–632
86. Johnson ER, Keinan S, Mori-Sánchez P, Contreras-García J, Cohen AJ, Yang W (2010) Revealing noncovalent interactions. J Am Chem Soc 132:6498–6506